A Sensorless I-F Start-up Strategy for Flying Start of Ultra-high-speed Permanent Magnet Motors based on Short-circuit Transient Differentiation

Wei Chen, *Member, IEEE*, Peizhe Liu, Lixiang Zhu, Xinmin Li, *Member, IEEE*, and Zhezhun Xu

***Abstract*—Conventional current-to-frequency (I-F) start-up strategies apply only to zero-speed conditions. When a nonzero initial speed (referred to as a flying start) exists, loss of synchronism is likely to occur because the virtual synchronous reference frame fails to align with the rotor flux linkage direction. To meet the flying start requirements of ultra-high-speed permanent magnet motors, this paper proposes a sensorless I-F start-up strategy for flying starts based on differential analysis of short-circuit transients. Upon power-up, the inverter places the three-phase stator windings in a controlled short-circuit state and applies two short-duration short-circuit pulses at different instants. By sampling the phase variation of the stator current vectors during the two short-circuit transients, differential current characteristics are extracted to rapidly estimate the initial rotor position and speed, thereby facilitating smooth I-F start-up. The proposed method overcomes the limitations of conventional I-F strategies confined to zero-speed start-up and is applicable to oil-film and air-bearing supported motor systems. Experimental results validate a smooth flying start featuring continuous and impact-free stator currents, effective suppression of mechanical friction prior to air-film formation, and the enhanced stability and robustness of I-F start-up.**

***Index Terms*—Ultra-high-speed permanent magnet motor, Current-to-frequency (I-F) start-up, Flying start, Short-circuit transient, Sensorless control.**

Manuscript received January 27, 2026; revised March 08, 2026; accepted March 23, 2026. Date of publication June 25, 2026. Date of current version April 17, 2026.

This work was supported by Zhejiang Province Pioneer Project under Grant 2024C01014), the Joint Fund Key Project of the National Natural Science Foundation of China under Grant U23A20643), and the National Natural Science Foundation of China under Grant 52477060).

Wei Chen is with the School of Electrical Engineering, Tiangong University, Tianjin 300387, China and also with the Zhejiang University Advanced Electrical Equipment Innovation Center, Hangzhou 311107, China (e-mail: chen_wei@tju.edu.cn).

Peizhe Liu and Xinmin Li are with the School of Electrical Engineering, Tiangong University, Tianjin 300387, China (e-mail: liupeizhe@tiangong.edu.cn; lixinmin@tju.edu.cn).

Lixiang Zhu is with the School of Control and Mechanical Engineering, Tianjin Chengjian University, Tianjin 300384, China (e-mail: zhulixiang@tcu.edu.cn).

Zhezhun Xu is with Technical Center of Hangzhou Customs, Hangzhou, 310007, China (email: xzz@zaiq.org.cn).

(*Corresponding Author: Xinmin Li*)

Digital Object Identifier 10.30941/CESTEMS.2026.00012.

I. INTRODUCTION

ULTRA-HIGH-SPEED permanent magnet synchronous motor (UHSPMSM) features high power density, high efficiency, and a compact structure, and has been widely applied in electric-assisted turbochargers and fuel cell air compressors [1]-[5].

With the development of non-contact bearing technology, the bearings have evolved from rolling bearings to air and oil film bearings [6]-[8], enabling low-friction and lubrication-free operation at ultra-high speeds. However, in practical engineering applications, the motor is often not at a complete standstill during shutdown or fault recovery stages. For instance, exhaust gas disturbances in electric-assisted turbocharging systems and rotor inertial coasting after a transient power loss both contribute to the motor having an initial rotor speed when power is restored. At low speeds, when the bearing film or oil film is not fully established, improper start-up control can easily lead to friction and impact between the rotor and bearing, causing film damage, mechanical wear, and system instability. Therefore, investigating sensorless start-up control methods under flying start operation is of significant importance.

For sensorless start-up control, UHSPMSM typically adopts three start-up strategies: high-frequency signal injection [9]-[10], voltage-to-frequency (V-F) control, and current-to-frequency (I-F) control. The high-frequency signal injection method relies on rotor magnetic anisotropy characteristics and is more suitable for an interior permanent magnet synchronous motor (IPMSM) with pronounced saliency. The subject of this study is the surface-mounted permanent magnet synchronous motor (SPMSM), which has weaker rotor magnetic anisotropy, making it difficult to obtain effective high-frequency response signals and therefore unsuitable for the high-frequency injection method. V-F control maintains a constant V-F ratio to preserve the magnetic flux amplitude, with a simple structure but uncontrollable current and poor disturbance immunity [11]. I-F start-up control introduces closed-loop regulation in the current loop while keeping the frequency open-loop, resulting in higher stability and torque control accuracy in the low-speed range [12]-[14]. In sensorless control, I-F start-up control applies a reference q-axis current i_q^* in a virtual synchronous rotating coordinate system to drive the motor from standstill to a certain speed.

This allows the motor to quickly cross the back-electromotive force (back-EMF) detection dead zone and the critical speed region of ultra-high-speed motors, ensuring full establishment of the back-EMF amplitude and creating conditions for subsequent closed-loop sensorless control. Therefore, I-F start-up control has become a key technology for establishing electromagnetic synchronization in sensorless ultra-high-speed drive systems.

However, conventional I-F start-up strategies are only applicable to standstill start-up. These strategies assume an initial rotor speed of zero and complete synchronization between the virtual synchronous reference frame and the rotor magnetic poles [15]. When the motor operates under flying start operation, conventional I-F start-up control is no longer applicable. In this case, a significant phase deviation $\Delta\theta$ arises between the virtual magnetic field and the rotor magnetic flux, leading to electromagnetic torque reversal or cancellation. This phase mismatch can cause current surges, speed oscillations, and even bearing film damage, preventing smooth start-up of the system. Therefore, conventional I-F start-up strategies exhibit significant limitations under flying start operation.

Furthermore, for sensorless start-up control under flying start operation, existing studies commonly employ closed-loop sensorless control methods after start-up, such as sliding-mode observer (SMO) [16]-[19], extended state observer (ESO) [20]-[21], and others. These methods collect stator voltage and current signals in real-time and estimate the back-EMF vector online based on the motor model, from which the rotor speed and position are inferred to achieve closed-loop synchronization control without position sensors. However, for UHSPMSM, back-EMF is approximately proportional to rotor speed. When the initial rotor speed is less than 10%-20% of the rated value, the back-EMF amplitude is small, and the waveform is significantly distorted. Back-EMF-based closed-loop observers are highly sensitive to noise and parameter mismatches, leading to estimation delays and oscillations. The back-EMF signal is insufficient to support stable observation, making closed-loop control unreliable in such conditions. Forcing the closed-loop control in this situation often results in estimation drift, current surges, and torque fluctuations, which can cause loss of synchronization and system instability, further compromising the stability of oil-film or air-bearing films. Therefore, traditional closed-loop sensorless control methods are difficult to maintain stable operation when starting with a low initial rotor speed, making this a major technical bottleneck for achieving reliable start-up in UHSPMSM.

To address the above issues, this paper proposes a sensorless I-F start-up strategy for flying start based on short-circuit transient differentiation. The method applies two short-duration short-circuit excitations sequentially at the instant of flying start. By analyzing the differential characteristics of the stator current transient responses, the initial rotor speed and position are rapidly estimated, and the estimated results are directly used as the initial parameters for I-F start-up control, enabling a seamless transition from transient identification to open-loop I-F operation. The proposed I-F start-up strategy for a flying start retrieves initial state information through short-circuit transients and performs open-loop I-F driving based on this information. Thus, it does not rely on back-EMF signals to achieve deterministic electromagnetic output when initial speed exists. This ensures a smooth start-up before the air bearing film is fully formed and provides predictable transient responses during bus voltage restoration, thereby establishing reliable initial conditions for subsequent closed-loop switching. The proposed strategy ensures both the feasibility of a flying start in practical engineering and the accuracy advantages of closed-loop control, making it particularly suitable for high-reliability flying start applications in oil-film bearing and air-bearing UHSPMSM systems.

The main research content and structure of this paper are as follows: Section II analyzes conventional I-F start-up strategies and their limitations; Section III derives the rotor speed and position estimation model based on short-circuit transient differentiation and presents the proposed I-F start-up strategy for flying start; Section IV validates the effectiveness of the proposed strategy through experiments conducted on a DSP28335-based platform; Section V summarizes the research work and discusses the potential application of the proposed strategy in high-reliability start-up systems for oil-film and air-bearing UHSPMSM.

II. Conventional I-F Start-up Strategy and Its Limitations

A. Mathematical Model of Permanent Magnet Synchronous Motor

The mathematical model of SPMSM in the d-q reference frame is considered in this section. By neglecting iron loss and magnetic saturation effects, the stator voltage equations can be expressed as:

$$\begin{bmatrix} u_\mathrm{d} \\ u_\mathrm{q} \end{bmatrix} = \begin{bmatrix} R_\mathrm{s} + pL_\mathrm{d} & 0 \\ 0 & R_\mathrm{s} + pL_\mathrm{q} \end{bmatrix} \begin{bmatrix} i_\mathrm{d} \\ i_\mathrm{q} \end{bmatrix} + \omega_\mathrm{e} \begin{bmatrix} -L_\mathrm{q} i_\mathrm{q} \\ L_\mathrm{d} i_\mathrm{d} + \psi_\mathrm{f} \end{bmatrix} \tag{1}$$

where u_d and u_q are the d-axis and q-axis stator voltages, respectively; i_d and i_q are the d-axis and q-axis stator currents, respectively. For SPMSM, the stator inductances satisfy $L_\mathrm{d} = L_\mathrm{q} = L_\mathrm{s}$. R_s and ψ_f denote the stator resistance and the permanent magnet flux linkage, respectively. p denotes the differential operator, and ω_e is the electrical angular speed.

The electromagnetic torque (T_e) can be expressed as:

$$T_\mathrm{e} = \frac{3}{2} n_\mathrm{p} \left(\psi_\mathrm{f} i_\mathrm{q} + \left(L_\mathrm{d} - L_\mathrm{q} \right) i_\mathrm{d} i_\mathrm{q} \right) \tag{2}$$

where n_p is the number of rotor pole pairs.

Since $L_\mathrm{d} = L_\mathrm{q}$ for SPMSM, the reluctance torque component can be neglected, and (2) can be simplified as:

$$T_\mathrm{e} = \frac{3}{2} n_\mathrm{p} \psi_\mathrm{f} i_\mathrm{q} \tag{3}$$

The mechanical motion equilibrium equation of the motor is given by:

$$T_\mathrm{e} - T_\mathrm{L} = J \frac{\mathrm{d}\omega_\mathrm{m}}{\mathrm{d}t} + B\omega_\mathrm{m} \tag{4}$$

where T_L is the load torque, J is the rotor moment of inertia, B

is the viscous damping coefficient, and ω_m is the mechanical angular speed.

B. Principle of Conventional I-F Start-up Control

To ensure stable motor operation during the start-up stage and to avoid current surges or loss of synchronization caused by unknown initial rotor position, conventional I-F start-up control typically performs a pre-positioning procedure before start-up. By injecting a stationary stator magnetomotive force (MMF) vector with a well-defined direction into the stator, an electromagnetic alignment torque T_e is generated, which forces the rotor magnetic poles to rotate toward the predetermined direction and eventually be attracted to and held at the designated position. This process usually aligns the d-axis of the rotor permanent magnet with the stator magnetic field, as illustrated in Fig. 1, thereby providing a reliable initial position reference for subsequent I-F start-up control.

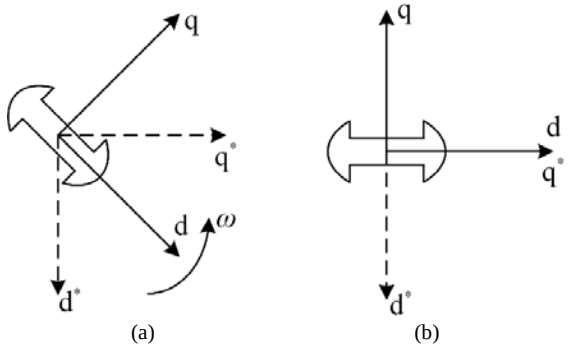

Fig. 1. Schematic diagram of rotor pre-positioning. (a) Initial state. (b) Completion of pre-positioning.

After the pre-positioning process is completed, the system enters the I-F start-up stage. In the virtual synchronous rotating reference frame d^*-q^*, the controller assigns the current commands $i_d^* = 0$ and a constant i_q^*, while the virtual magnetic field rotates at the prescribed electrical angular frequency ω_e^*.

According to (1), when the angular speed of the virtual reference frame ω_e^* equals ω_e, the stator-induced EMF and the permanent magnet back-EMF remain spatially balanced. Under this condition, electromagnetic power transfer becomes stable, and the system enters synchronous steady-state operation. The steady-state stator current and electromagnetic torque are given by:

$$i_q = i_q^* \tag{5}$$

$$T_e = \frac{3}{2} n_p \psi_f i_q^* \tag{6}$$

To gradually establish magnetic flux and electromagnetic torque from standstill, I-F start-up increases the motor speed by applying an electrical angular frequency ramp command:

$$\omega_e^*(t) = kt \tag{7}$$

where k is the frequency ramp rate and t denotes time.

To prevent loss of synchronization caused by excessive step changes in the electrical frequency, the frequency ramp rate is typically determined offline according to the load characteristics and control requirements. The current magnitude is usually set to a constant value i_q^*, thereby forming a linear "current-frequency" coupling and enabling smooth motor start-up. This control strategy does not rely on position or speed feedback and exhibits favorable stability in the zero-speed and low-speed operating regions.

C. Limitations of Conventional I-F Start-up Strategy Under Flying Start

1) Torque Reversal and Instability Caused by Phase Deviation

Under flying start operation, conventional I-F start-up control still assumes that the initial motor speed is zero and establishes the current-frequency command based on the virtual magnetic field rotating at the electrical angular speed ω_e^*. However, in this case, the rotor magnetic flux continues to rotate at the actual electrical angular speed $\omega_e = n_p\omega_m$. As a result, an initial angular deviation exists between the virtual magnetic field and the rotor magnetic flux.

$$\Delta\theta = \theta_e^* - \theta_e \tag{8}$$

where θ_e^* denotes the rotor position in the virtual synchronous rotating reference frame, and θ_e represents the actual rotor position of the motor.

When $\Delta\theta$ exists between the virtual d^*-q^* reference frame and the actual rotor magnetic flux, the current transformation relationship can be expressed as:

$$\begin{bmatrix} i_d \\ i_q \end{bmatrix} = \begin{bmatrix} \cos\Delta\theta & \sin\Delta\theta \\ -\sin\Delta\theta & \cos\Delta\theta \end{bmatrix} \begin{bmatrix} i_d^* \\ i_q^* \end{bmatrix} \tag{9}$$

During start-up, $i_d^* = 0$; therefore, it follows that:

$$i_d = -i_q^* \sin\Delta\theta \tag{10}$$

$$i_q = i_q^* \cos\Delta\theta \tag{11}$$

By substituting the above relationship into (3), the electromagnetic torque can be expressed as:

$$T_e(\Delta\theta) = \frac{3}{2} n_p \psi_f i_q^* \cos\Delta\theta \tag{12}$$

It can be observed that the electromagnetic torque exhibits a cosine relationship with the phase deviation. When $|\Delta\theta|$ is small, the torque experiences only slight attenuation. As $|\Delta\theta|$ approaches $\pi/2$, the start-up torque decreases significantly, and the system becomes prone to loss of synchronization. When $|\Delta\theta| > \pi/2$, the magnetic field polarities are interleaved, resulting in torque reversal, which may cause reverse rotation or oscillatory behavior of the motor.

2) Current Distortion Caused by Back-EMF Coupling

According to (1), the stator voltage contains the back-EMF term $\omega_e\psi_f$. When the motor is started under flying start operation, the back-EMF vector can be expressed as:

$$\boldsymbol{E} = \omega_e P \boldsymbol{\Psi}_r \tag{13}$$

where $\boldsymbol{\Psi}_r$ is the rotor flux linkage vector with a magnitude of ψ_f, and P denotes a 90° rotation operator, indicating that the back-EMF vector $\boldsymbol{E}$ is always orthogonal to the rotor flux linkage $\boldsymbol{\Psi}_r$.

If the controller still generates the stator voltage command $\boldsymbol{u}_s^*$ based on the zero-speed model, the stator current at the instant of start-up ($\boldsymbol{i}_s$) can be approximately expressed as:

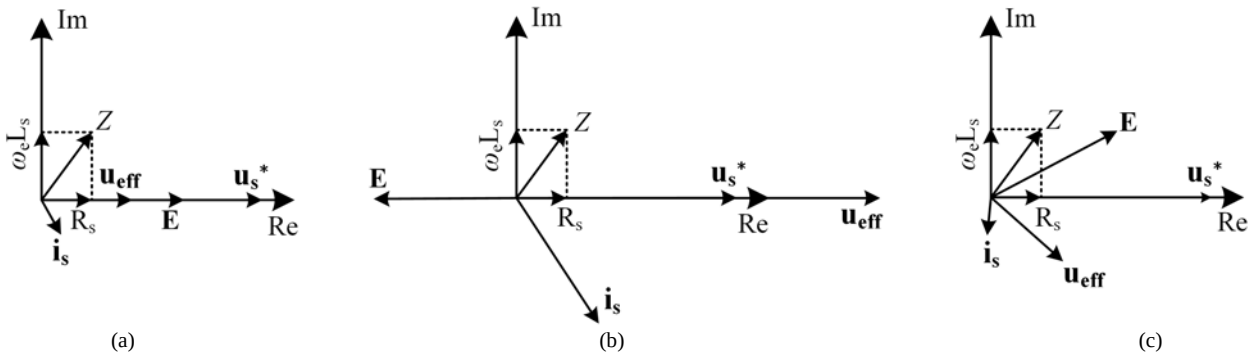

Fig. 2. Current response characteristics caused by the phase difference between stator voltage and back-EMF. (a) $\Delta\theta = 0°$. (b) $\Delta\theta = 180°$. (c) $0 < \Delta\theta < 180°$.

$$\boldsymbol{i}_s \approx \frac{\boldsymbol{u}_{eff}}{Z} = \frac{\boldsymbol{u}_s^* - \boldsymbol{E}}{R_s + j\omega_e L_s} \tag{14}$$

where $\boldsymbol{u}_{eff}$ denotes the equivalent effective stator voltage space vector, Z represents the equivalent stator impedance, and L_s denotes the stator inductance.

When $\boldsymbol{u}_s^*$ is in phase with the back-EMF vector $\boldsymbol{E}$, the two components partially cancel each other, reducing the effective stator voltage magnitude and causing a rapid collapse of the stator current. Conversely, when they are in anti-phase, the voltage components are superimposed, leading to a sharp increase in the stator current and resulting in electromagnetic shock. In the general case, where the phase difference $\Delta\theta$ lies within the range 0 to π, the stator voltage and back-EMF are nonlinearly superimposed in space. As a consequence, both the magnitude and phase of the stator current vector vary with time, introducing additional alternating fluctuation components. In a three-phase system, these fluctuations manifest as current magnitude imbalance and harmonic distortion, which in turn induce transient instability of the system and, in severe cases, lead to loss of synchronization and start-up failure. Fig. 2 illustrates the current response characteristics caused by the phase difference between stator voltage and back-EMF.

In summary, under flying start operation, conventional I-F start-up strategies suffer from torque reversal and instability caused by phase deviation, as well as current distortion induced by back-EMF coupling. These issues pose a serious threat to system stability and reliable motor operation.

III. I-F START-UP STRATEGY FOR FLYING START BASED ON SHORT-CIRCUIT TRANSIENT DIFFERENTIATION

To address the aforementioned limitations, this paper proposes a sensorless I-F start-up strategy for flying start based on short-circuit transient differentiation. In the initial stage of start-up, a short-duration controlled short-circuit excitation is applied. The proposed method exploits the differential characteristics of the transient short-circuit current responses to reflect the initial rotor motion state: When the rotor is at standstill, no short-circuit current response is observed, whereas with nonzero initial speed, a significant transient short-circuit current response is exhibited. Based on this characteristic, the proposed approach can distinguish between standstill start-up and flying start operation without requiring additional decision criteria. Furthermore, under flying start operation, the initial rotor speed and position can be rapidly estimated, enabling a smooth I-F start-up.

A. I-F Start-up Control Procedure for Flying Start

The I-F start-up control procedure for flying start based on short-circuit transient differentiation is illustrated in Fig. 3. S_1, S_3, and S_5 denote the upper-arm switching signals of the three-phase inverter, while S_2, S_4, and S_6 denote the corresponding lower-arm switching signals. i_{scp} represents the peak phase current generated during the short-circuit interval, whose magnitude is smaller than the rated stator phase current.

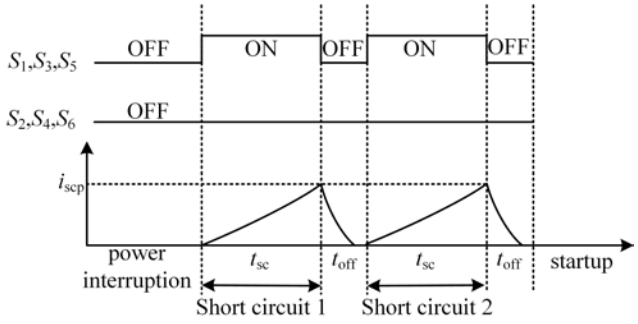

Fig. 3. I-F start-up procedure for flying start based on short-circuit transient differentiation.

When the motor is in a freewheeling or residual rotating state prior to start-up, the controller employs short-circuit transient differentiation to identify the initial operating state. This method excites and compares the transient responses of the short-circuit currents through two successive stator winding short-circuit operations. The procedure is described as follows. First, a three-phase short circuit is applied immediately after flying start to excite the short-circuit current. After a predefined duration t_{sc}, the phase current is sampled, and the inverter bridge is turned off, allowing the current to decay naturally. Subsequently, after an interval t_{off}, a second short-circuit operation is performed, and the sampling process is repeated.

By calculating the differential characteristics of the two short-circuit current transients, the rotation direction of the rotor flux linkage and the initial electrical angular speed can be accurately inferred, thereby enabling estimation of the initial rotor speed and position. After the current naturally decays, synchronous I-F start-up control for flying start is completed based on the estimated initial states.

B. Speed and Position Estimation based on Short-circuit Transient Differentiation

In this section, two short-duration short-circuit excitations are applied to extract the initial rotor state information by exploiting the differential characteristics of the transient current responses. Rotor rotation induces phase variation in the stator current, and analysis of the differential current responses provides an initial synchronization basis for I-F start-up for flying start.

1) Current Sampling and Analysis under Short-circuit Excitation

As illustrated in Fig. 3, after the power supply is restored, the controller immediately applies a short circuit to the three-phase stator windings and maintains it for a duration t_{sc}. During this interval, the stator windings generate short-circuit current driven by the back-EMF, and the current magnitude rises rapidly. At $t = t_{sc}$, the controller samples the three-phase currents to obtain the first sampled current vector $\boldsymbol{I}_{sc1}$. After performing the 3/2 coordinate transformation, the phase angle of this sampled current vector at $t = t_{sc}$ with respect to the α-axis of the α-β reference frame (or equivalently, the A-phase axis of the three-phase stator coordinate system) can be determined:

$$\theta_1 = \text{atan2}\left(i_{\beta1}, i_{\alpha1}\right) \tag{15}$$

where $i_{\alpha1}$ and $i_{\beta1}$ denote the components of the first set of sampled currents in the α-β coordinate system, and θ_1 represents the angle of the current vector with respect to the α-axis.

After the first short-circuit operation is completed, the controller turns off all switching devices of the inverter bridge, allowing the three-phase stator currents to decay naturally. Once the currents decrease to zero, a second short-circuit operation is applied to the stator windings, with its duration also set to t_{sc}. By sampling the three-phase currents at the end of the second short-circuit interval, the second sampled current vector $\boldsymbol{I}_{sc2}$ can be obtained. The phase angle of $\boldsymbol{I}_{sc2}$ at $t = t_{sc}$ with respect to the α-axis of the α-β reference frame (or equivalently, the A-phase axis of the three-phase stator coordinate system) can be expressed as:

$$\theta_2 = \text{atan2}\left(i_{\beta2}, i_{\alpha2}\right) \tag{16}$$

where $i_{\alpha2}$ and $i_{\beta2}$ denote the components of the second set of sampled currents in the α-β coordinate system, and θ_2 represents the angle of the current vector with respect to the α-axis.

2) Speed and Position Estimation based on Short-circuit Transient Differentiation

The time interval between the two current sampling instants is $t_{sc} + t_{off}$. Under the condition that $\omega_e(t_{sc} + t_{off}) < \pi$, the variation of the electrical angular speed during this interval can be considered sufficiently small. Moreover, considering the pronounced inertia of the UHSPMSM rotor system, the influence of mechanical losses on the electrical angular speed can be neglected within the extremely short duration ($t_{sc} + 2t_{off}$). Therefore, the initial electrical angular speed of the motor can be approximated as being equal to the average electrical angular speed over this interval:

$$\omega_{e0} = \overline{\omega_e} = \frac{\theta_2 - \theta_1}{t_{sc} + t_{off}} \tag{17}$$

Therefore, the initial speed of the motor at start-up is:

$$n_0 = \frac{30\omega_{e0}}{n_p \pi} \tag{18}$$

Under short-circuit conditions, the stator voltage satisfies:

$$u_d = u_q = 0 \tag{19}$$

Additionally, since the short-circuit duration t_{sc} is much smaller than the time constant of the motor's q-axis stator winding L_q/R_s, the stator resistance R_s can be approximated as $R_s \approx 0$ during the short-circuit period. Therefore, based on (1) and (17), the dynamic equations of the dq-axis current during the short-circuit period can be derived as follows:

$$\begin{bmatrix} 0 \\ 0 \end{bmatrix} = \begin{bmatrix} pL_s & 0 \\ 0 & pL_s \end{bmatrix} \begin{bmatrix} i_d \\ i_q \end{bmatrix} + \omega_{e0} \begin{bmatrix} -L_s i_q \\ L_s i_d + \psi_f \end{bmatrix} \tag{20}$$

By differentiating the dynamic equation of the d-axis current and substituting it into the dynamic equation of the q-axis current, the second-order ordinary differential equation for i_d can be obtained:

$$\frac{d^2 i_d}{dt^2} + \omega_{e0}^2 i_d = -\omega_{e0}^2 \frac{\psi_f}{L_s} \tag{21}$$

By considering the initial conditions $i_d(0) = i_q(0) = 0$ under short-circuit conditions, the above differential equation is solved to obtain the analytical solution for the short-circuit current i_d:

$$i_d(t) = -\frac{\psi_f}{L_s}\left(1 - \cos \omega_{e0} t\right) \tag{22}$$

By further substituting $i_d(t)$ into the dynamic equation of the d-axis current, the analytical solution for the q-axis current can be obtained:

$$i_q(t) = -\frac{\psi_f}{L_s} \sin \omega_{e0} t \tag{23}$$

Therefore, at the short-circuit moment $t = t_{sc}$, we have:

$$\begin{bmatrix} i_d(t_{sc}) \\ i_q(t_{sc}) \end{bmatrix} = \begin{bmatrix} -\frac{\psi_f}{L_s}\left(1 - \cos \omega_{e0} t_{sc}\right) \\ -\frac{\psi_f}{L_s} \sin \omega_{e0} t_{sc} \end{bmatrix} \tag{24}$$

From (24), the angle between I_{sc2} and the d-axis can be calculated as:

$$\theta_{sc} = \arctan\left(\frac{\sin\left(\omega_{e0} t_{sc}\right)}{1 - \cos\left(\omega_{e0} t_{sc}\right)}\right) \tag{25}$$

As illustrated in Fig. 4, the rotor position angle at the second current sampling instant satisfies:

$$\theta_2' = \theta_2 - \theta_{sc} \tag{26}$$

where θ_2' represents the rotor position angle at the instant of the second current sampling, and θ_{sc} represents the angle between the current vector $\boldsymbol{I}_{sc2}$ and the d-axis during the short-circuit period.

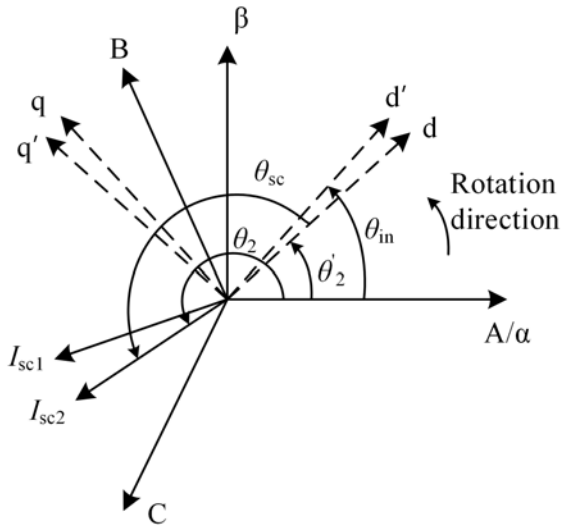

Fig. 4. Vector diagram of short-circuit transient differential current.

The initial rotor position θ_{in} at the start-up instant corresponds to the rotor position obtained by advancing θ'_2 over the interval t_{off}. According to (26), it can be obtained as:

$$\theta_{in} = \theta'_2 + \omega_{e0} t_{off} \tag{27}$$

Through (15)-(27), the rotor speed and position can be obtained at the initial stage of start-up by means of short-circuit transient differentiation, thereby achieving initial synchronization for I-F start-up control for flying start. The proposed strategy involves low computational burden and fast estimation, and is suitable for I-F start-up processes under nonzero initial speed operation.

Based on the above mathematical model and control principle, the block diagram of the I-F start-up control system for flying start can be established, as illustrated in Fig. 5.

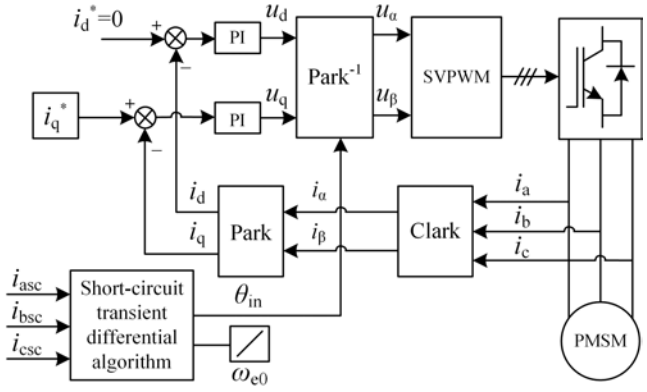

Fig. 5. Block diagram of the I-F start-up control system for flying start.

3) Parameter Design Guidelines and Stability Analysis

The selection of the short-circuit excitation duration t_{sc} and the short-circuit interval t_{off} requires a trade-off between signal observability and system safety.

At the short-circuit instant $t = t_{sc}$, the magnitude of the stator phase current is:

$$i_{scp} = \sqrt{i_d(t_{sc})^2 + i_q(t_{sc})^2} \tag{28}$$

From (24), (25), and (28), the functional relationship between the peak stator phase current and the electrical angular speed can be obtained as:

$$i_{scp} = \psi_f \sqrt{\left(\frac{1-\cos\omega_{e0}t_{sc}}{L_d}\right)^2 + \left(\frac{\sin\omega_{e0}t_{sc}}{L_q}\right)^2} \tag{29}$$

Based on (29), the duration of the short-circuit excitation t_{sc} can be determined: If t_{sc} is too short, the change in current amplitude is not significant, leading to an increased estimation error of the initial state. Conversely, if t_{sc} is too long, it can cause excessive current amplitude, potentially damaging the motor or power devices. Additionally, the value of t_{sc} varies depending on the flying start operation. In this paper, for the start-up experiments under flying start operation of 6000 r/min, t_{sc} = 400 μs, and for the start-up experiments under flying start operation of 3000 r/min, t_{sc} = 900 μs.

The selection of the short-circuit interval t_{off} should ensure sufficient decay of the stator current so as to avoid coupling between the two short-circuit transients. In this study, the current decay process is assumed to follow an exponential decay model:

$$i(t) = i_{scp} e^{-\frac{t}{\tau}} \tag{30}$$

where τ denotes the current decay time constant, which is determined by the motor's resistance, stator inductance, and other parameters.

In the experiment, it is necessary to ensure that the current decays to zero after the t_{off} period. Additionally, to ensure the accuracy of the initial electrical angular velocity estimation, the condition $\omega_e(t_{sc} + t_{off}) < \pi$ must also be satisfied. Based on the above constraints, in this paper, t_{off} is set to a fixed value of 100 μs, which does not change with the flying start operation.

Since the short-circuit excitation duration is brief and the entire process occurs at the initial stage of start-up, the proposed method does not impose adverse effects on the overall system stability and is capable of providing reliable initial synchronization conditions for subsequent I-F start-up control. Therefore, under the aforementioned conditions, the appropriate selection of the short-circuit excitation duration and interval ensures stable operation of the system.

C. Synchronous Stability Control after I-F Start-up for Flying Start

Since I-F start-up control for flying start is an open-loop speed control scheme without a closed-loop speed feedback path, the motor speed cannot be self-regulated. Moreover, the damping coefficient B is entirely determined by the load characteristics, which are typically fixed; therefore, the damping coefficient can be regarded as constant during motor operation. When the load damping coefficient is small, the motor exhibits pronounced speed fluctuations and slow convergence, resulting in poor system stability. Consequently, compensation of the damping torque component of the motor system is required.

To address the instability of the I-F start-up control system for flying start, this paper adopts an active power feedback

control method to enhance the stability of the I-F start-up control for flying start [22]. In this approach, the motor voltage and current signals are measured in real time to calculate the instantaneous active power. A high-pass filter is then applied to the instantaneous active power to extract its high-frequency disturbance component. In this paper, the cutoff frequency of the high-pass filter is set to 2.58 Hz, which is determined based on the motor's mechanical oscillation characteristics and the dynamic response requirements of the control system. The filtered high-frequency disturbance component is then multiplied by a gain factor and fed back to the speed reference of the I-F start-up control for flying start, enabling real-time adjustment of the reference electrical angular speed ω_e^*. By regulating the speed reference, the system damping ratio is increased, leading to improved motor stability. The corresponding block diagram is shown in Fig. 6.

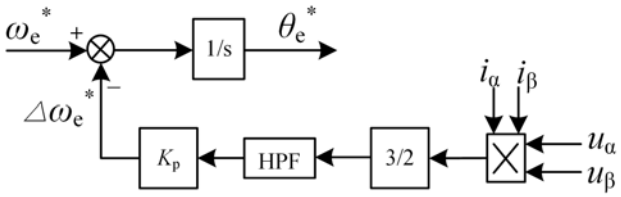

Fig. 6. Block diagram of the active power feedback control scheme.

By analyzing the simplified model of UHSPMSM, it can be shown that the system damping torque can be increased by applying a speed disturbance suppression component that is proportional to the disturbance of the rotor electrical angular speed $\Delta\omega_e$ and opposite in direction, thereby improving the speed convergence characteristics of the motor. The speed disturbance suppression component is expressed as:

$$\Delta\omega_e^* = -K_p \frac{d\Delta\omega_e}{dt} \tag{31}$$

where K_p is the proportional coefficient.

The value of K_p is inversely proportional to the reference electrical angular speed ω_e^*:

$$K_p = \frac{const}{\omega_e^*} \tag{32}$$

Since the sensorless control method adopted in this paper cannot accurately obtain the rotor position and speed information in the low-speed region, the disturbance of the instantaneous active power ΔP_m is used to approximately replace the disturbance of the rotor electrical angular speed $\Delta\omega_e$. The corresponding relationship is expressed as:

$$\frac{d\Delta\omega_e}{dt} \propto \Delta P_m \tag{33}$$

The disturbance of the active power ΔP_m can be replaced by the variation of the input power P_e:

$$\Delta P_m = \Delta P_e = \mathrm{HPF}\left(\frac{3}{2}\left(u_\alpha i_\alpha + u_\beta i_\beta\right)\right) \tag{34}$$

From (12), it can be observed that $\Delta\theta$ varies with T_L. Accordingly, the fluctuation in the electromagnetic torque output ΔT_e caused by $\Delta\omega_e^*$ can be expressed as:

$$\Delta T_e = -\frac{3}{2} n_p \psi_f i_q^* \cos\Delta\theta \Delta\omega_e^* \tag{35}$$

From (35), it can be seen that the electromagnetic torque variation ΔT_e generated by the active power feedback algorithm is proportional to $\Delta\omega_e^*$ and opposite in direction to the load torque.

By substituting (32)-(34) into (31), the speed disturbance suppression component can be expressed as:

$$\Delta\omega_e^* = -\frac{const}{\omega_e^*} \mathrm{HPF}\left(\frac{3}{2}\left(u_\alpha i_\alpha + u_\beta i_\beta\right)\right) \tag{36}$$

where HPF represents a high-pass filter, u_α and u_β are the stator voltage components in the α-β coordinate system, and i_α and i_β are the stator current components in the α-β coordinate system.

From the above analysis, it can be concluded that the rotor electrical angular speed ω_e varies with the load torque T_L, resulting in an electrical angular speed disturbance $\Delta\omega_e$. Through the action of the speed disturbance suppression component in (36), this disturbance is dynamically compensated in the virtual magnetic field angular speed ω_e^*, thereby forming a feedback regulation mechanism opposite to the disturbance direction. This process is equivalent to introducing additional damping into the system, which suppresses speed oscillations and accelerates speed convergence.

After compensation, the dynamic characteristics of the virtual magnetic field are modified, and the system generates a damping torque component as described in (35). This effectively increases the system damping coefficient, accelerates convergence and steady-state establishment during the start-up process, and realizes adaptive synchronization and stable control after flying start.

IV. Experimental Validation and Results Analysis

A. Experimental Platform Setup

To verify the correctness of the theoretical analysis and the effectiveness of the proposed strategy, an experimental platform based on a UHSPMSM system was established. The experimental setup and the prototype motor are shown in Fig. 7. The experimental platform mainly consists of a core controller, a power module, a water-cooling unit, a digital oscilloscope, and the experimental prototype. The core controller employs a DSP (TMS320F28335) and an FPGA (EP1C6Q240C8) as the central control units. The power module is built around an intelligent power module (IPM) as the main power device. A water-cooling unit (MCW-15C/X1-06XZ-2385) is used for thermal management. The experimental system is powered by a Watson direct current (DC) power supply, and the experimental results are recorded using an eight-channel digital oscilloscope (DLM4058, Yokogawa, Japan) and a four-channel digital oscilloscope (DLM3024, Yokogawa, Japan). The experimental prototype is a 10-kW air compressor, and its detailed parameters are listed in Table I.

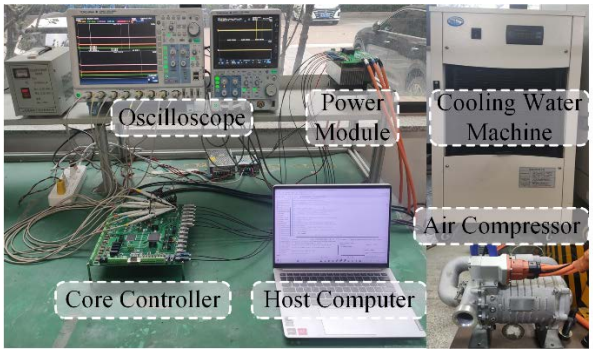

Fig. 7. Experimental system platform and prototype motor.

TABLE I
MOTOR PARAMETERS

Parameter	Value
Rated voltage, U_N/V	500
Rated current, I_N/A	14.1
Rated speed, n_N/(r·min^{-1})	60,000
Phase resistance, R/Ω	0.014
Phase inductance, L/mH	0.138
Flux linkage/Wb	0.00194
Motor inertia, J/(kg·m^2)	0.00008802
Pairs of poles, p	1

B. Experimental Results Analysis

The proposed UHSPMSM sensorless control system adopts a staged coordinated control strategy. During the initial start-up stage, open-loop I-F control is employed, in which the motor is accelerated by maintaining a constant current magnitude and applying a linear frequency ramp. The acceleration rate is set to 20,000 r/min per second, enabling rapid establishment of the air bearing. When the speed reaches 20,000 r/min, the control system, based on the torque-power angle self-equilibrium theory, reduces the q-axis current reference i_q^*, allowing the power angle to increase adaptively. During this process, the error angle $\Delta\theta$ between the I-F control and the rotor position estimated by the SMO gradually decreases. Once the error angle $\Delta\theta$ falls below the predefined threshold of 10°, the control system automatically switches to SMO-based closed-loop sensorless control, achieving rotor position synchronization and smooth transition. This threshold is determined through experimental tuning to ensure smooth control switching while avoiding current surges. The system then continues accelerating and ultimately reaches the rated speed of 60,000 r/min.

To verify the effectiveness of the proposed I-F start-up control strategy for flying start based on short-circuit transient differentiation, comparative experiments were conducted between conventional I-F control and the proposed I-F control for flying start. Two operating conditions with initial speeds of 6000 and 3000 r/min were tested, respectively.

Fig. 8 presents a comparison of experimental results between conventional I-F start-up control and the proposed I-F start-up control for flying start under an initial speed of 6000 r/min. Fig. 8(a) shows the results obtained using the conventional I-F start-up control, while Fig. 8(b) corresponds to the proposed I-F start-up control for flying start based on short-circuit transient differentiation.

Fig. 8(a) includes the estimated rotor position, rotor speed, three-phase stator current, and the q-axis current waveforms. Although the motor eventually starts successfully, pronounced speed fluctuations and oscillations are observed during the start-up process. The estimated rotor position signal exhibits abrupt variations and jitter, and significant distortion and amplitude fluctuation in the stator currents are evident during start-up. In particular, during the speed synchronization process, the three-phase stator currents show strong asymmetry and high-frequency components, indicating that the conventional I-F start-up strategy struggles to ensure smooth start-up under nonzero initial speed operation. Furthermore, from the comparison of the actual q-axis current and the reference q-axis current waveforms, it can be observed that during the start-up phase, the actual q-axis current exhibits significant overshoot and oscillations, making it difficult to stabilize and track the reference value. This suggests substantial fluctuations in the current regulation process, leading to unstable electromagnetic torque output. In this scenario, the distorted currents cause an uneven electromagnetic force distribution between the stator and rotor, resulting in considerable electromagnetic vibrations and axial impacts. These effects impose additional load and wear on the air or oil-film bearings, accelerating bearing fatigue and degradation, and significantly reducing the operational lifetime and reliability of the motor system.

Fig. 8(b) shows the waveforms of the estimated rotor position and the initial rotor position, the estimated speed and the initial speed, the three-phase stator currents, as well as the q-axis current. As shown in the zoomed view (Zoom1), a certain deviation exists between the initial rotor position θ_{in} and the position estimated by the SMO, θ_{smo}. Further observation from Zoom5 indicates that a discrepancy also exists between the initial speed n_0 and the SMO-estimated speed n_{smo}. These deviations arise from the fact that, during the early stage of flying start, the back-EMF amplitude is relatively small, making it difficult for the SMO to accurately extract effective back-EMF information from the current variations, thereby degrading its position and speed estimation accuracy. This limitation is inherent to the observer under low-speed operation rather than to the proposed method itself. In addition, during the short-circuit transient differentiation stage, a transient jump in the SMO-estimated position can be observed in Zoom1. This phenomenon is caused by the rapid change in stator current at the instant of switching between the two short-circuit operations, to which the SMO is highly sensitive due to its dependence on current derivatives, resulting in short-lived estimation fluctuations.

Nevertheless, as shown by the three-phase stator current waveforms, the three-phase current remains continuous and smooth at the moment of start-up, without any current surges or distortions, indicating that the system is able to establish stable electromagnetic torque. Additionally, from the comparison of the actual q-axis current and the reference q-axis current waveforms, it can be seen that under the proposed control strategy, the actual q-axis current tracks the reference

value quickly and smoothly, with no significant overshoot or oscillations. This further validates the stability of current regulation during the start-up process. Therefore, the proposed method effectively restores rotor position and speed, enabling stable I-F flying start operation and significantly enhancing the system's reliability and robustness.

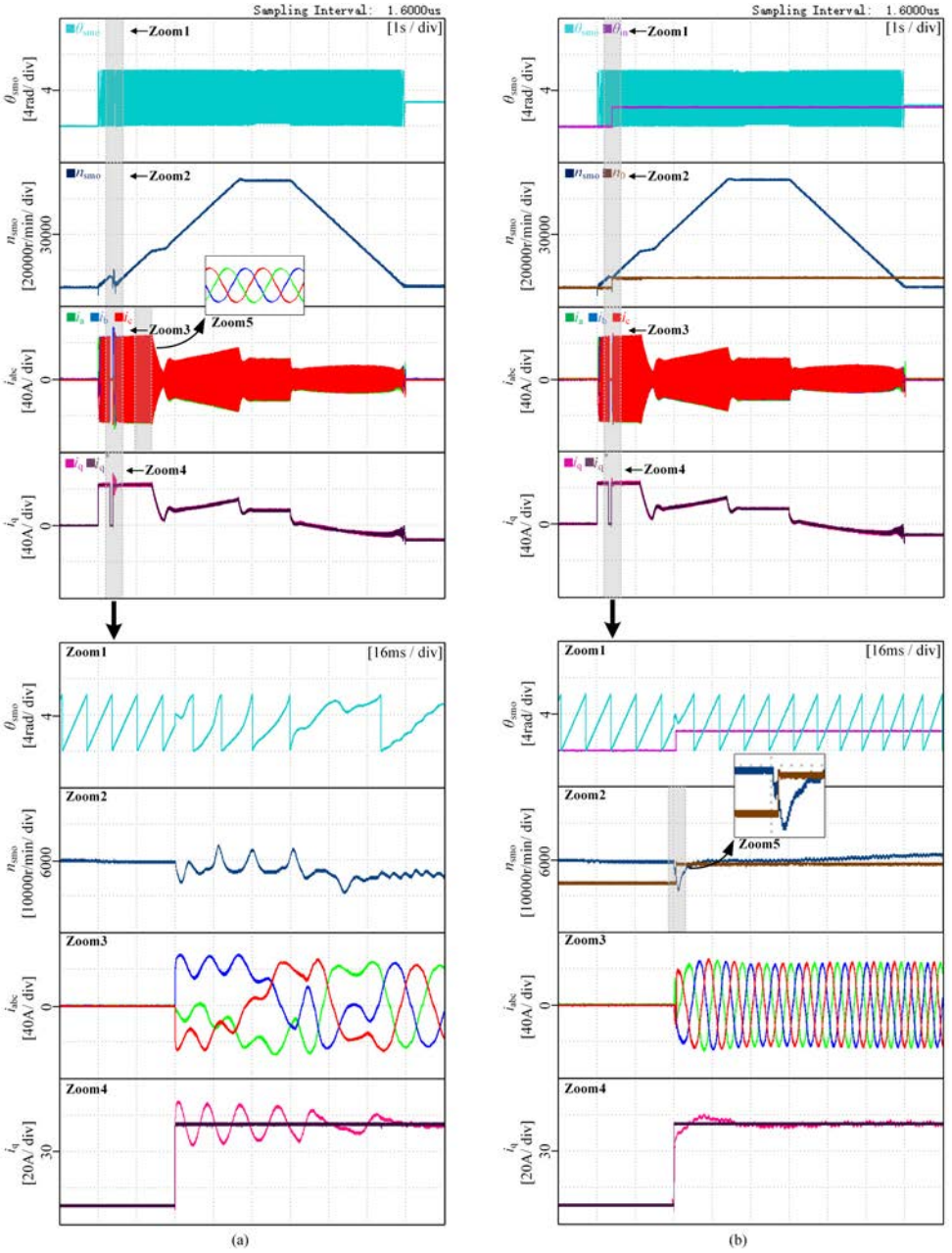

Fig. 8. Comparison of experimental results under an initial speed of 6000 r/min. (a) Conventional I-F start-up control. (b) Proposed I-F start-up control for flying start.

Fig. 9 shows the experimental results of the smooth transition from open-loop I-F control to SMO-based closed-loop control under an initial speed of 6000 r/min. Here, $\Delta\theta$ denotes the error angle between the rotor position under I-F control and that estimated by the SMO. The green waveform represents the switching completion flag F_{SC}. After the motor speed reaches 20,000 r/min, the q-axis current reference i_q^* is gradually reduced while maintaining an acceleration rate of 5000 r/min per second, allowing the error angle $\Delta\theta$ to decrease adaptively. Once $\Delta\theta$ falls below the predefined threshold, the control mode is switched, the flag F_{SC} is set to one, and the smooth transition to sensorless closed-loop control is completed.

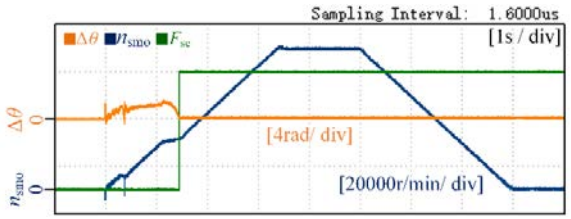

Fig. 9. Experimental results of smooth sensorless control transition under an initial speed of 6000 r/min.

Fig. 10 presents a comparison of experimental results between conventional I-F start-up control and the proposed I-F start-up control for flying start under an initial speed of 3000

r/min. Fig. 10(a) shows the results obtained using the conventional I-F start-up control, while Fig. 10(b) corresponds to the proposed I-F start-up control for flying start based on short-circuit transient differentiation.

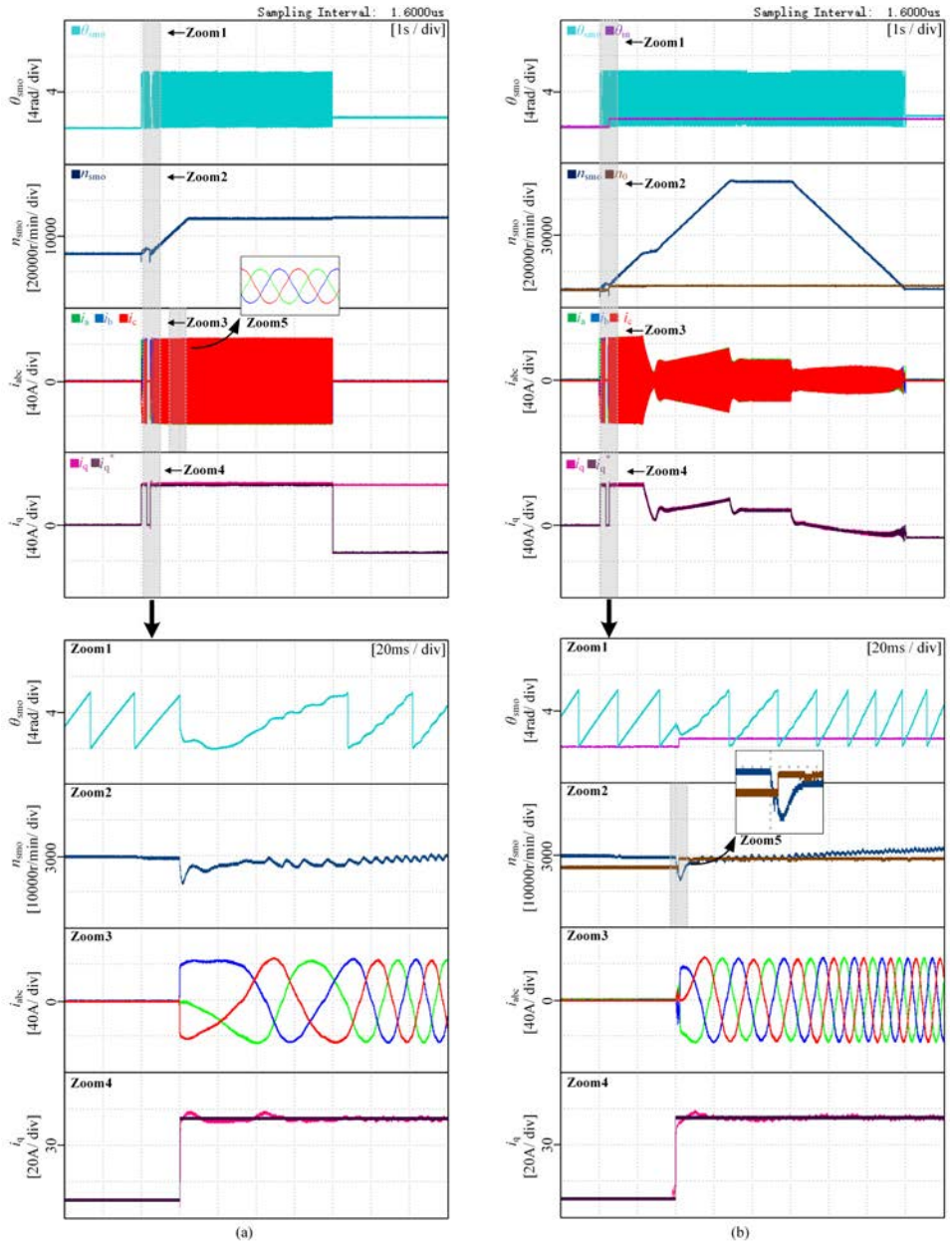

Fig. 10. Comparison of experimental results under an initial speed of 3000 r/min. (a) Conventional I-F start-up control. (b) Proposed I-F start-up control for flying start

As shown in Fig. 10(a), significant distortion appears in the three-phase stator current waveforms at the instant of power-on. To further assess the operating condition during this stage, a comparison between the zoomed waveform in Zoom5 of Fig. 10(a) and the corresponding waveform during successful start-up in Zoom5 of Fig. 8(a) reveals that, during the start-up process shown in Fig. 8(a), the three-phase stator currents exhibit slight distortion and phase modulation due to back-EMF coupling. In contrast, in Fig. 10(a), the current waveforms during the corresponding interval show ideal sinusoidal shapes, with nearly constant amplitude and perfect three-phase symmetry, without any phase drift or envelope variation caused by back-EMF. This indicates that the motor's rotor has essentially stopped rotating during this stage, and the stator current is primarily generated by the electromagnetic excitation applied by the control system. Furthermore, from the waveform in Zoom4 of Fig. 10(a), it can be seen that although the actual q-axis current oscillation is minimal, the q-axis current remains at a high level without dropping after flying start operation. This suggests that the control system failed to achieve the expected transition from start-up to steady-state operation. Therefore, it can be concluded that, under these operating conditions, the motor lost synchronization and entered the purely electromagnetic excitation stage, with the mechanical speed rapidly decaying to zero during this process. However, the estimated speed signal shows a temporary increase in this stage. This phenomenon arises because, when the rotor is stationary, the open-loop I-F control

continues to inject a rotating stator voltage at the prescribed electrical frequency, causing continuous rotation of the stator flux. When calculating the back-EMF, the SMO primarily tracks the flux rotation induced by the control command rather than the actual rotor motion. As a result, this virtual electromagnetic variation is misinterpreted as mechanical acceleration, leading to an overestimation of the rotor speed.

As shown in Fig. 10(b), during the initial stage of start-up, further reduction in rotor speed results in certain estimation errors in both the SMO-estimated rotor position θ_{smo} and the estimated speed n_{smo}. However, the three-phase stator current waveforms remain continuous at the flying start instant, without current surges or distortion. At the same time, the actual q-axis current is able to track the reference value well throughout the entire operation. This demonstrates that the proposed strategy can achieve smooth synchronization and stable start-up under flying start operation, exhibiting strong robustness and practical applicability.

Fig. 11 shows the experimental results of the smooth transition from open-loop I-F control to SMO-based closed-loop control under an initial speed of 3000 r/min. After rapid reconstruction of the rotor position and speed, a smooth transition from open-loop I-F control to SMO closed-loop control is achieved. Throughout the entire switching process, the electromagnetic state of the system remains continuous, and the dynamic response is stable. This demonstrates that the coordination between I-F control and SMO-based closed-loop control is reliable, enabling stable start-up under flying start operation.

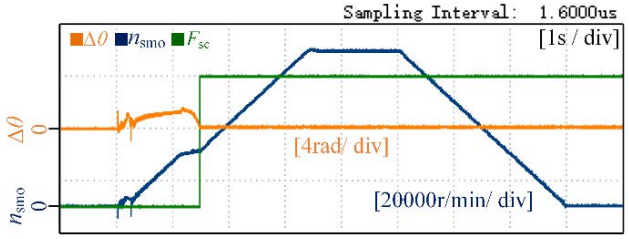

Fig. 11. Experimental results of smooth sensorless control transition under an initial speed of 3000 r/min.

In summary, conventional I-F control exhibits evident limitations under flying start operation. Its open-loop frequency modulation mechanism is unable to accurately match the initial rotor position and speed, which easily leads to current distortion and even loss of synchronization. For ultra-high-speed permanent magnet motor systems, this issue not only reduces the start-up success rate but also adversely affects bearing stability and overall system reliability. In contrast, the proposed I-F start-up strategy for flying start maintains continuous and distortion-free stator current waveforms during the start-up process, achieving smooth start-up and synchronized stable control under flying start operation. These results verify the effectiveness and robustness of the proposed strategy for flying start applications.

V. Conclusion

This paper addresses the limitations of conventional I-F start-up control, which is applicable only to zero-speed operation and is prone to current surges and loss of synchronization during flying start. A sensorless I-F start-up strategy for flying start of ultra-high-speed permanent magnet motors based on short-circuit transient differentiation is proposed. The main conclusions are summarized as follows:

1) The proposed strategy successfully achieves smooth I-F start-up for flying start under nonzero initial speed operation. Stable and reliable operation can be maintained even under low back-EMF amplitude and high distortion operation, overcoming the limitation of conventional I-F start-up strategies that are restricted to zero-speed operation.

2) The proposed strategy enables rapid synchronization and stable start-up at initial speeds of 3000 and 6000 r/min, with smooth and impact-free stator current waveforms, thereby verifying its robustness and engineering feasibility.

3) The proposed strategy is particularly suitable for oil-film and air-bearing UHSPMSM systems subjected to frequent start-stop operation and flying start operation. It effectively reduces the risks of bearing film collapse and rotor wear, thereby enhancing the safety and reliability of start-stop operation.

In conclusion, the proposed I-F start-up strategy for flying start based on short-circuit transient differentiation achieves fast sensorless identification and smooth start-up control under nonzero initial speed operation, demonstrating strong engineering practicality and potential for wide application.

References

[1] M. S. Lim, J. M. Kim, and Y. S. Hwang *et al*., "Design of an Ultra-high-speed Permanent-magnet Motor for an Electric Turbocharger Considering Speed Response Characteristics," *IEEE/ASME Trans. on Mechatronics*, vol. 22, no. 2, pp. 774-784, Apr. 2017.

[2] J. X. Shen, X. F. Qin, and Y. C. Wang, "High-speed Permanent Magnet Electrical Machines—applications, Key Issues and Challenges," *CES Trans. on Electr. Mach. and Syst.*, vol. 2, no. 1, pp. 23-33, Mar. 2018.

[3] H. J. Zhang, W. F. Yu, and W. Hua, "Design and Key Technology of Oil-free Centrifugal Air Compressor for Hydrogen Fuel Cell," *CES Trans. on Electr. Mach. and Syst.*, vol. 6, no. 1, pp. 11-19, Mar. 2022.

[4] H. Lin, X. Wei, and H. P. Geng *et al*., "Performance Analysis on High-speed Permanent Magnet Motor Used in Air Compressor of Hydrogen Fuel Cells," in *Proc. of 2024 6th Int. Conf. on Power and Energy Technol*., Beijing, China, Jul. 2024, pp. 487-492.

[5] T. W. Lee, D. K. Hong, and T. U. Jung, "High-speed, High-power Motor Design for a Four-legged Robot Actuator Optimized Using the Weighted Sum and Response Surface Methods," *CES Trans. on Electr. Mach. and Syst*., vol. 5, no. 3, pp. 224-231, Sept. 2021.

[6] Z. Li, K. Yang, and X. T. Wang, "Characteristics Analysis of PM Multi-DOF Motor with Air Bearing Structure," in *Proc. of 2020 IEEE Int. Conf. on Appl. Supercond. and Electromagn. Devices*, Tianjin, China, Oct. 2020, pp. 1-2.

[7] W. Tsunoda, A. Chiba, and T. Shinshi, "Vibration Control for a Rotor Supported by Oil-film Bearings Using a Bearingless Motor," *IEEE/ASME Trans. on Mechatronics*, vol. 24, no. 3, pp. 1368-1375, Jun. 2019.

[8] W. Tsunoda, A. Chiba, and T. Shinshi, "Combination of Oil Film Bearing and Bearingless Motor for High Load Capacity and Stable Rotation," in *Proc. of 2018 IEEE 27th Int. Symp. on Ind. Electron*., Cairns, QLD, Australia, Jun. 2018, pp. 120-125.

[9] X. M. Li, Y. Yan, and Y. M. Xu *et al*., "Low-speed Rotating Restart and Speed Recording for Free-running Sensorless IPMSM based on Ultrahigh Frequency Sinusoidal Wave Injection," *IEEE Trans. on Power Electron.*, vol. 37, no. 12, pp. 15245-15259, Dec. 2022.

[10] T. Wu, D. R. Luo, and S. Huang *et al*., "A Fast Estimation of Initial

Rotor Position for Low-speed Free-running IPMSM," *IEEE Trans. on Power Electron.*, vol. 35, no. 7, pp. 7664-7673, Jul. 2020.

[11] Z. Y. Tang, X. Li, and S. Dusmez *et al*., "A New V/f-based Sensorless MTPA Control for IPMSM Drives," *IEEE Trans. on Power Electron.*, vol. 31, no. 6, pp. 4400-4415, Jun. 2016.

[12] H. Kim, J. Song, and K. Lee, "Q-MRAS based I-F Startup for Model Predictive Current Controlled Sensorless SPMSM Drive," *IEEE Trans. on Ind. Appl.*, vol. 61, no. 6, pp. 9394-9403, Nov.-Dec. 2025.

[13] D. Z. Chen, K. Y. Lu, and D. Wang *et al*., "I-F Control with Zero D-axis Current Operation for Surface-mounted Permanent Magnet Synchronous Machine Drives," *IEEE Trans. on Power Electron.*, vol. 38, no. 6, pp. 7504-7513, Jun. 2023.

[14] J. L. Xing, Z. D. Qin, and C. Lin *et al*., "Research on Startup Process for Sensorless Control of PMSMs based on I-F Method Combined with an Adaptive Compensator," *IEEE Access*, vol. 8, pp. 70812-70821, Apr. 2020.

[15] Z. H. Song, W. X. Yao, and K. Lee *et al*., "An Efficient and Robust I-f Control of Sensorless IPMSM with Large Startup Torque based on Current Vector Angle Controller," *IEEE Trans. on Power Electron.*, vol. 37, no. 12, pp. 15308-15321, Dec. 2022.

[16] L. F. Gou, C. C. Wang, and M. L. Zhou *et al*., "Integral Sliding Mode Control for Starting Speed Sensorless Controlled Induction Motor in the Rotating Condition," *IEEE Trans. on Power Electron.*, vol. 35, no. 4, pp. 4105-4116, Apr. 2020.

[17] W. Chen, L. X. Zhu, and S. Wang *et al*., "Rotating Restart Method for TPFS Inverter-fed Sensorless PMSM Drive System based on Dual Effective Voltage Vectors Injection," *IEEE Trans. on Power Electron.*, vol. 39, no. 9, pp. 11708-11722, Sept. 2024.

[18] F. Jukić, L. Pravica, and D. Sumina *et al*., "Framework for Sensorless Control and Flying Start of a Permanent Magnet Generator based on a Sliding Mode Observer," *IEEE Trans. on Ind. Electron.*, vol. 71, no. 1, pp. 294-304, Jan. 2024.

[19] C. C. Wang, L. F. Gou, and S. F. Dong *et al*., "Sensorless Control of IPMSM based on Super-twisting Sliding Mode Observer with CVGI Considering Flying Start," *IEEE Trans. on Transp. Electrification*, vol. 8, no. 2, pp. 2106-2117, Jun. 2022.

[20] F. Du, Z. Liu, and J. Li *et al*., "Restart Strategy for Sensorless Control of Permanent Magnet Synchronous Motor in Flux-weakening Region," *IEEE Trans. on Transp. Electrification*, vol. 11, no. 5, pp. 11243-11254, Oct. 2025.

[21] D. W. Seo, Y. Bak, and K. B. Lee, "An Improved Rotating Restart Method for a Sensorless Permanent Magnet Synchronous Motor Drive System Using Repetitive Zero Voltage Vectors," *IEEE Trans. on Ind. Electron.*, vol. 67, no. 5, pp. 3496-3504, May 2020.

[22] F. Haichao, S. Boyang, and G. Lizhen, "A Closed-loop I/f Vector Control for Permanent Magnet Synchronous Motor," in *Proc. of 2017 9th Int. Conf. on Modelling, Identification and Control*, Kunming, China, Jul. 2017, pp. 965-969.

Wei Chen (Member, IEEE) was born in Shanxi, China, in 1977. He received the B.S., M.S., and Ph.D. degrees in electrical engineering from Tianjin University, Tianjin, China, in 2000, 2003, and 2006, respectively.

He is currently a Professor with the School of Electrical Engineering, Tiangong University, Tianjin, and a researcher with the Zhejiang University Advanced Electrical Equipment Innovation Center, Hangzhou, and the Vice President with the National Local Joint Engineering Research Center of Electric Machine System Design and Manufacturing, China. His research interests include electrical machines and drives, power electronics.

Peizhe Liu was born in Henan, China, in 2000. He received the B.S. degree in electrical engineering and automation from Henan University of Technology, Henan, China, in 2023.

He is currently working toward the M.S. degree in electrical engineering from Tiangong University, Tianjin, China. His research interests include electrical machines, motor drives, and power electronics.

Lixiang Zhu was born in Hebei, China, in 1997. He received the M.S. degree in electrical engineering and the Ph.D. degree in control science and engineering from Tiangong University, Tianjin, China, in 2022 and 2025, respectively. He is currently a Lecturer with the School of Control and Mechanical Engineering, Tianjin Chengjian University, Tianjin, China.

His research interests include electrical machines, motor drives, and power electronics.

Xinmin Li (Member, IEEE) was born in Hunan, China, in 1989. He received the B.S. degree in automation from University of Science and Technology Beijing, Beijing, China, in 2011, and the Ph.D. degree in electrical engineering from Tianjin University, Tianjin, China, in 2017.

He is currently a Professor with the Zhejiang University Advanced Electrical Equipment Innovation Center, and also with the School of Electrical Engineering, Tiangong University, Tianjin, China. His research interests include electrical machines and motor drives, electric drive systems of electric vehicles, power electronics, and wind power technology.

Zhezhun Xu was born in Zhejiang Province, China, in 1969. He received the B.S. degree in Electrical Machines in 1990, the M.S. degree in Theoretical Electrical Engineering in 1993, and the Ph.D. degree in Power Electronics in 1997, all from Zhejiang University, China.

He is currently a Researcher with the Technical Center of Hangzhou Customs, where he is engaged in safety performance testing of mechanical and electrical products. His research interests include electrical machines and drives, electromagnetic fields, and power electronics.